

Thermal Plumes and Convection in Highly Compressible Fluids

Yuhei Chiwata and Akira Onuki

Department of Physics, Kyoto University, Kyoto 606-8502, Japan
(Received 5 March 2001; published 11 September 2001)

We present simple hydrodynamic equations of supercritical fluids close to the gas-liquid critical point. We numerically solve them to examine plume generation and convection under gravity. These results are in good agreement with the experiment [A. B. Kogan and H. Meyer, Phys. Rev. E **63**, 056310 (2001)]. This Letter is a first study of transient behavior of convection, which is unique in compressible fluids due to the piston effect.

DOI: 10.1103/PhysRevLett.87.144301

PACS numbers: 44.25.+f, 47.27.Te, 64.70.Fx

As the critical point is approached in supercritical fluids, the compressibility and thermal expansion grow, and hence thermal and mechanical disturbances are inseparably coupled. In such fluids the thermal diffusion constant D is very small, while the pressure propagation is rapid. As a result, adiabatic processes are of great importance [1]. A characteristic feature not expected in incompressible fluids is that the density heterogeneity is much more exaggerated than that of the temperature due to strong enhancement of the thermal expansion coefficient $\alpha_p = -(\partial\rho/\partial T)_p/\rho$.

We mention some salient effects of supercritical fluid hydrodynamics. First, we note that thermal equilibration processes drastically depend on whether the pressure or the volume of the fluid is fixed. This is because the thermal diffusion layer near the boundary wall of the fluid container acts as a *piston* causing instantaneous adiabatic changes in the interior region in the fixed volume condition (the piston effect) [2–6]. This piston is so effectively operative near the critical point that it decisively influences isochoric thermal relaxations. Second, an expanded region with excess entropy created around a heater can have a long lifetime due to slow thermal diffusion. In gravity it will eventually rise upward as a thermal *plume* as visualized experimentally [5,7] and numerically [8]. Third, as $T \rightarrow T_c$, there is a crossover in the mechanism of convection in the Rayleigh-Bénard geometry from the usual one for incompressible fluids to that of the Schwarzschild criterion [9,10]. In the usual case, convection occurs when the Rayleigh number $\text{Ra} \equiv \alpha_p \rho_c g L^3 \Delta T / \eta D$ exceeds the critical value $\text{Ra}_c (\cong 1708)$ [11]. Here ΔT is the difference between the bottom and top temperatures, L is the cell width, η is the viscosity, and D is the thermal diffusivity. In the latter criterion, convection is triggered when thermal plumes continue to rise upward adiabatically. This occurs when the applied temperature gradient $|dT/dz|$ is larger than the adiabatic gradient [12],

$$a_g \equiv (\partial T / \partial p)_s \rho g, \quad (1)$$

which is equal to 0.034 mK/cm for ${}^3\text{He}$ near the critical point. The effective temperature gradient seen by rising plumes is given by $|dT/dz| - a_g$. Now the convection onset for compressible fluids is given by $\text{Ra}^{\text{corr}} > \text{Ra}_c$, where Ra^{corr} is a corrected Rayleigh number defined by [9]

$$\text{Ra}^{\text{corr}} = \text{Ra}(1 - a_g L / \Delta T). \quad (2)$$

Thus $(\Delta T)_{\text{onset}} = a_g L + \text{Ra}_c (D \eta / g \rho \alpha_p L^3)$ at the onset. In near-critical fluids, very large Ra can be realized [13–15], and the crossover between the two criteria was detected in SF_6 from velocity measurements [13] and has recently been investigated from $(\Delta T)_{\text{onset}}$ with precision in ${}^3\text{He}$ [16,17]. The aim here is to present simple hydrodynamic equations of supercritical fluids and show numerical results of convection.

Let a supercritical fluid on the critical isochore be in a cell with the bottom plate at $z = 0$ and the top plate at $z = L$. The total fluid volume is fixed at V . We assume that the temperature disturbance $\delta T(\mathbf{r}, t) = T(\mathbf{r}, t) - T_{\text{top}}$ measured from the temperature T_{top} at the top boundary is much smaller in magnitude than $T_{\text{top}} - T_c$. Hereafter the distance from the critical point is measured by $\epsilon \equiv T_{\text{top}} / T_c - 1$. We also assume that the gravity-induced density stratification is not too severe such that the thermodynamic derivatives are nearly homogeneous in the cell. This is satisfied when $|\rho / \rho_c - 1| \sim (\partial \rho / \partial p)_T g L \ll \epsilon^\beta$ [18]. Thus we assume

$$\epsilon^{\beta+\gamma} > a_g L / T_c, \quad (3)$$

where $\beta \cong 0.33$ and $\gamma \cong 1.24$ are the critical exponents. In equilibrium the pressure gradient is given by $-\rho g \cong -\rho_c g$. In nonequilibrium we set

$$p(\mathbf{r}, t) = p_0 - \rho_c g z + p_1(t) + p_{\text{inh}}(\mathbf{r}, t), \quad (4)$$

where p_0 is a constant, $p_1(t)$ and p_{inh} are the homogeneous and inhomogeneous parts induced by δT , respectively. Here we assume $\langle p_{\text{inh}} \rangle = 0$, where $\langle \dots \rangle \equiv \int d\mathbf{r}(\dots) / V$ represents the space average. Using the thermodynamic relation $dp = (\partial p / \partial T)_\rho dT + (\partial p / \partial \rho)_T d\rho$ and the condition that the space average of the density deviation vanishes, we find [2]

$$p_1(t) = (\partial p / \partial T)_\rho \langle \delta T \rangle(t). \quad (5)$$

It is important that the combination $p(\mathbf{r}, t) + \rho_c g z$ is nearly homogeneous or $|p_1(t)| \gg |p_{\text{inh}}(\mathbf{r}, t)|$ for fluid motions much slower than L/c ($c \sim 10^4$ cm/s being the sound velocity) [1]. The entropy $s(\mathbf{r}, t)$ per unit mass consists of the equilibrium part $s_{\text{eq}}(z)$ with $ds_{\text{eq}}/dz =$

$-(\partial s/\partial p)_T \rho g = T^{-1} C_p a_g$ and the nonequilibrium deviation, $\delta s(\mathbf{r}, t) \equiv T^{-1} C_p [\delta T(\mathbf{r}, t) - (\partial T/\partial p)_s p_1(t)]$. With the aid of the thermodynamic identity $(\partial T/\partial p)_s = (\partial T/\partial p)_\rho (1 - 1/\gamma_s)$, the heat conduction equation, $\rho T(\partial/\partial t + \mathbf{v} \cdot \nabla) s = \lambda \nabla^2 \delta T$, is rewritten as [1]

$$\left(\frac{\partial}{\partial t} + \mathbf{v} \cdot \nabla - D \nabla^2 \right) \delta T = (1 - \gamma_s^{-1}) \frac{d}{dt} \langle \delta T \rangle - a_g v_z, \quad (6)$$

where $D = \lambda/\rho C_p$ with λ being the thermal conductivity, and $\gamma_s = C_p/C_V$ is the specific heat ratio. Here $C_p \sim \epsilon^{-\gamma}$ and $C_V \sim \epsilon^{-\alpha}$ are the specific heats at constants p and V , respectively, with $\alpha \cong 0.1$. The first term on the right-hand side of Eq. (6) arises from $p_1(t)$, leading to the piston effect [2]. The second term arises from ds_{eq}/dz and suppresses the upward motion of plumes.

On long time scales ($\gg L/c$), sound waves decay to zero and the incompressibility condition $\nabla \cdot \mathbf{v} = 0$ becomes nearly satisfied. The time scale of the velocity field is then given by $L^2 \rho/\eta$ in terms of the viscosity η . Another characteristic feature is that the Prandtl number $\text{Pr} \equiv \eta/\rho D$ increases in the critical region; for example, $\text{Pr} = 350$ at $T/T_c - 1 = 10^{-3}$ in ${}^3\text{He}$. This means that the time scale of the thermal diffusion is much longer than that of the velocity. In the low-Reynolds number condition $\text{Re} < 1$ we may use the equation for the momentum rate change in the Stokes approximation,

$$\eta \nabla^2 \mathbf{v} = \nabla p + g \rho \mathbf{e}_z \cong \nabla p_{\text{inh}} - \alpha_p \rho_c g \delta T \mathbf{e}_z, \quad (7)$$

where \mathbf{e}_z is the unit vector along the z axis. We note that an inhomogeneity of δT changing perpendicularly to the z axis induces an incompressible flow. Let k be the typical wave number (or $2\pi/k$ be the typical length) of the fluid motion and $(\delta T)_c$ be the typical temperature variation in the xy plane. Then the magnitude of the velocity field is of the order $(\alpha_p \rho_c g / \eta k^2) (\delta T)_c$ and $\text{Re} \sim \rho |\mathbf{v}| / \eta k \sim (\alpha_p \rho_c^2 g / \eta^2 k^4) (\delta T)_c$. For convection we set $kL \sim 2\pi$ and $(\delta T)_c \sim \Delta T - (\Delta T)_{\text{onset}}$ and rewrite the condition $\text{Re} < 1$ as

$$\text{Ra}^{\text{corr}}/\text{Ra}_c - 1 < \text{Pr}. \quad (8)$$

Thus Eq. (7) is valid in a considerably wide range of Ra^{corr} for $\text{Pr} \gg 1$. In addition, Eq. (7) yields $p_{\text{inh}} \sim \alpha_p \rho_c g L (\delta T)_c \sim \epsilon^{-\gamma} \rho_c g L (\delta T)_c / T_c$. Using Eq. (5) we have $|p_{\text{inh}}| \ll |p_1(t)|$ in the temperature region where Eq. (3) is valid, unless $\langle \delta T \rangle$ is much smaller than the characteristic size of δT .

For a steady convection pattern, we set $\delta T(\mathbf{r})/\Delta T = 1 - z/L + \mathcal{F}(L^{-1}\mathbf{r})/\text{Ra}$. The dimensionless function \mathcal{F} vanishes at $z = 0$ and L and obeys

$$\mathbf{V} \cdot \tilde{\nabla} \mathcal{F} = \tilde{\nabla}^2 \mathcal{F} + \text{Ra}^{\text{corr}} V_z, \quad (9)$$

where $\tilde{\nabla} = L\nabla$ is the space derivative in units of L . The dimensionless velocity $\mathbf{V} = (L/D)\mathbf{v}$ obeys $\tilde{\nabla}^2 \mathbf{V} = \tilde{\nabla} p_{\text{inh}} - \mathcal{F} \mathbf{e}_z$, where p_{inh} ensures $\tilde{\nabla} \cdot \mathbf{V} = 0$. At the convection onset we thus obtain $\text{Ra}^{\text{corr}} = \text{Ra}_c$ [9,10]. The efficiency of convective heat transport is represented

by the Nusselt number $\text{Nu} \equiv QL/\lambda\Delta T$, where Q is the heat flux through the cell. For steady convection we have

$$\text{Nu} = 1 + \text{Ra}^{-1} f_\lambda(\text{Ra}^{\text{corr}}), \quad (10)$$

where $f_\lambda = -L(\partial \mathcal{F}/\partial z)_{z=0}$ is a function of Ra^{corr} . Consistently with this result [19], experimental curves of $\text{Ra}(\text{Nu} - 1)$ vs $\text{Ra}^{\text{corr}}/\text{Ra}_c - 1$ were collapsed onto a single universal curve for various densities above T_c [14] and for various ϵ on the critical isochore [16].

Using the same conditions as in the experiments [16,17], we perform a numerical analysis of Eqs. (6) and (7) in two dimensions for ${}^3\text{He}$ at $\epsilon = 0.05$ in a cell with $L = 1.06$ mm, where $\gamma_s = 22.8$, $T\alpha_p = 26.9$, $D = 5.42 \times 10^{-5}$ cm²/s, and $\text{Pr} = 7.4$. The condition (3), $\epsilon > 2 \times 10^{-4}$, is well satisfied. In this case we have $\text{Ra}^{\text{corr}}/\text{Ra}_c = 0.90[\Delta T/a_g L - 1]$ with $a_g L = 3.57$ μK . The convection occurs for $\Delta T > 7.6$ μK . We impose the periodic boundary condition in the lateral direction with period $4L$. We apply a constant heat flux at the bottom for $t > 0$ with a fixed top temperature; then, the bottom temperature is a function of time. The boundary temperature deviations are independent of the lateral coordinates and $\Delta T(t) \equiv T_{\text{bot}} - T_{\text{top}}$ is a function of time only. In our simulation the one-dimensional pattern with $\mathbf{v} = \mathbf{0}$ becomes linearly unstable against perturbations with period $2L$ for $Q > 16$ nW/cm² and also against those with period $4L/3$ for $Q > 40$ nW/cm². We integrate Eq. (6) on a 400×100 lattice assigning a small random number to the initial value of δT at each lattice point. In our cell with width $4L$ we then have two pairs of rolls, with each pair having a $2L$ period, for $16 < Q < 42$ nW/cm² and three pairs of rolls with $4L/3$ period for larger Q in the final steady state [20]. Note that the roll period is known to be $2.02L$ slightly above the onset for infinite lateral dimension [11], while the aspect ratio was 57 in the experiments.

In Fig. 1 we plot time evolution of the temperature difference $\Delta T(t)$ for various Q . When convection sets in, an overshoot and a subsequent damped oscillation of ΔT follow. As shown in the inset of Fig. 1, the same transient behavior was observed in the experiment [17]. Figure 2 shows the numerically obtained curve for $Q = 45.8$ nW/cm² (solid line), which nearly coincides with the theoretical curve (dotted curve) without convection for $t \leq 22$ s. The latter curve is obtained from Eq. (6) with $\mathbf{v} = \mathbf{0}$. As shown in Fig. 3 the early-stage temperature profile is strongly influenced by the piston effect at fixed volume for $t > t_1 = L^2/D(\gamma_s - 1)^2 = 0.42$ s [2]. The peak height and the amplitude of the oscillation in our simulation are somewhat larger than the experimental ones. This difference could originate from the fact that we realize only roll-like plumes in two dimensions, while plumes should be more easily ejected from the bottom in three dimensions. In Fig. 2 we also show that the overshoot and damped oscillation become much weaker at fixed pressure, in which the first term on the right-hand side of Eq. (6) is

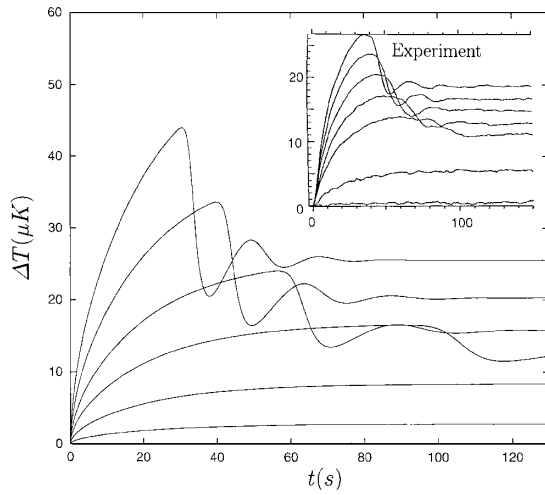


FIG. 1. Numerical results of $\Delta T(t)$ vs time after application of heat flux Q from the bottom, where the top temperature is fixed. Here $T/T_c - 1 = 0.05$, and $Q = 5, 15, 25, 45.8, 70,$ and 100 nW/cm^2 from below. The experimental curves [17] are shown in the inset, where $Q = 0.65, 9.22, 36.6, 45.8, 55.2,$ and 64.3 nW/cm^2 from below.

absent. In the steady state at long times, the numerical results of $\Delta T(\infty)$ vs Q agree well with the experimental data, as shown in Fig. 4 [20].

Figure 5 displays snapshots of the profiles of the temperature deviations at fixed volume. In 5(A) the profile is nearly one dimensional, while in 5(B) $\Delta T(t)$ attains a maximum. In 5(C) the cooler fluid region near the top begins to flow to the bottom with a velocity v . An excess cooling then occurs adiabatically, producing damped oscillation of δT in the whole space region. In 5(D) $\Delta T(t)$ has dropped to half of the peak value.

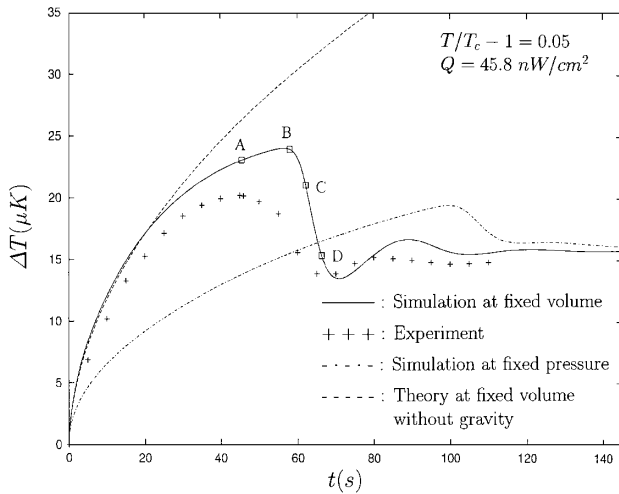


FIG. 2. Comparison between the numerical relaxation curve for three rolls at a $4L/3$ period (solid line) and the data (+) [17] of $\Delta T(t)$ vs time. Here $Q = 45.8 \text{ nW/cm}^2$ and the volume is fixed. The upper broken curve represents the theoretical one for $v = 0$ obtained from integration of Eq. (6). The dash-dotted curve represents the numerical curve with three rolls at fixed pressure. For the points (\square) the temperature profiles are given in Fig. 5.

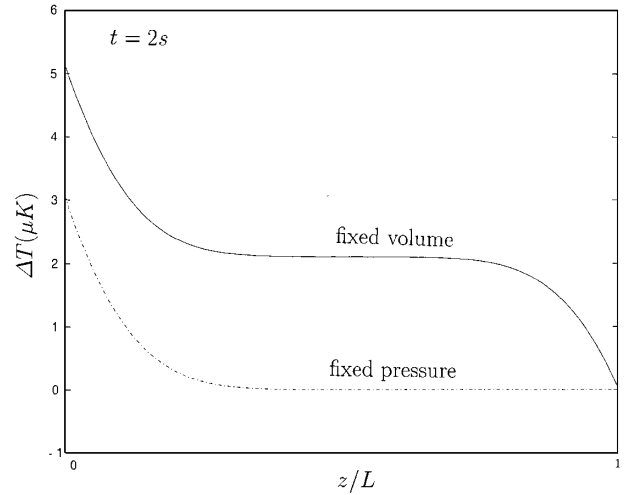


FIG. 3. The early-stage temperature profiles at $t = 2 \text{ s}$ at fixed volume and pressure conditions after application of heat flux at $t = 0$. The parameters are the same as in Fig. 2.

In 5(E) we show the steady state profile. Using the estimation of v below Eq. (7), the time t_m from 5(B) to 5(D) is estimated as $t_m \sim L/v \sim t_D / (\text{Ra}^{\text{corr}} / \text{Ra}_c - 1)$, where $t_D = L^2/4D = 52 \text{ s}$ is the diffusion time. This expression fairly explains the experimental data of t_m [21]. The time t_p at the peak is considerably longer than t_m . Both t_p and t_m grow as $\text{Ra}^{\text{corr}} \rightarrow \text{Ra}_c$. In addition, at fixed pressure, the roll pattern grows nearly monotonically into the final steady pattern. Finally we consider the Reynolds number Re , which we define as $\text{Re} = (\rho/\eta) \{ \int dr |v \cdot \nabla v|^2 / \int dr |\nabla^2 v|^2 \}^{1/2}$. In Fig. 5 the maximum of Re is 0.2 at 5(C). For $Q = 100 \text{ nW/cm}^2$, where $\text{Ra}^{\text{corr}} / \text{Ra}_c \sim 5.5 < \text{Pr} = 7.4$, the maximum of Re is increased to 0.6. This is consistent with Eq. (8). As Q is increased, plumes are generated and detached from the bottom on smaller space-time scales. Eventually for $\text{Ra}^{\text{corr}} / \text{Ra}_c > 10$ the temperature gradient becomes

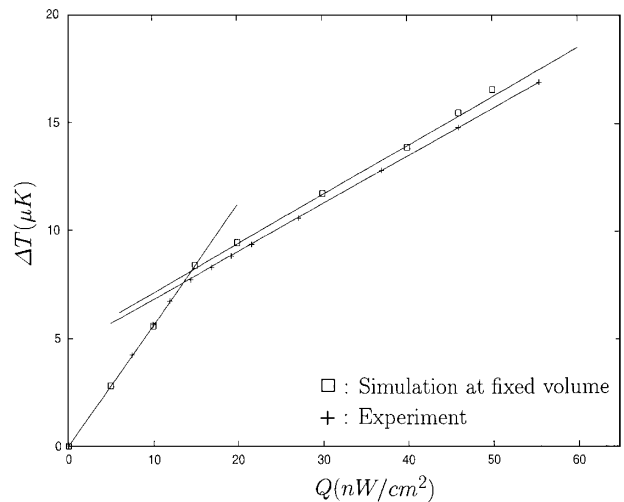


FIG. 4. The steady state ΔT vs heat flux Q . Here the points (\square) are our numerical results and those (+) are the experimental data [17].

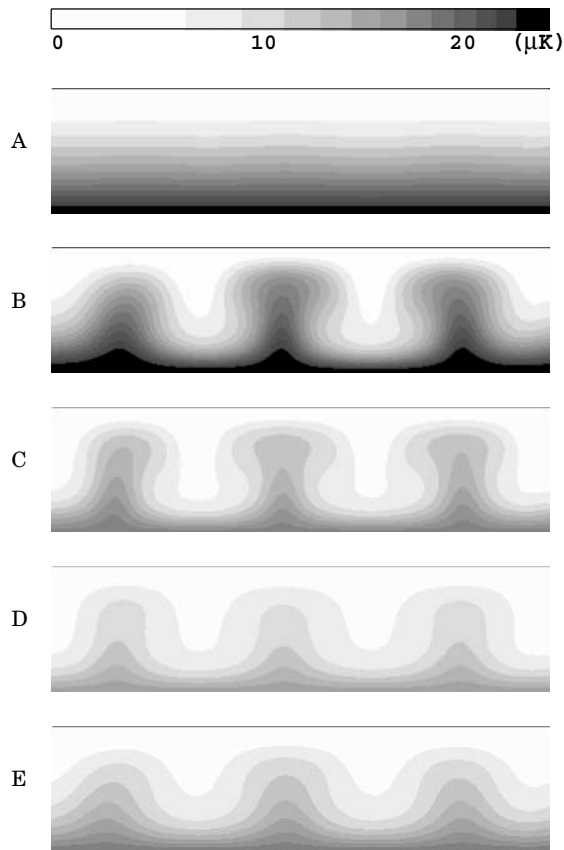


FIG. 5. Temperature profiles at (A), (B), (C), and (D), on the curve in Fig. 2 (\square). The bottom one (E) represents the steady profile. Here $\delta T = 0$ at the top boundary and $\delta T > 0$ below it. The δT at the bottom boundary is equal to ΔT .

localized near the bottom and top boundaries, resulting in the scaling behavior $Nu \sim (Ra^{\text{corr}}/Ra_c)^a$ with $a \cong 1/4$ in agreement with the experiment [17]. Work to extend simulations to larger values of Ra^{corr} and Re will appear shortly.

In summary, we properly take into account the piston effect and the adiabatic temperature gradient effect. Though performed in two dimensions, numerical solutions of our dynamic equations fairly agree with the experiment [17].

We thank Horst Meyer for valuable suggestions and comments. Thanks are also due to S. Amiroudine for informative correspondence. This work is supported by the Japan Space Forum Grant No. H12-264.

- [1] A. Onuki, *Phase Transition Dynamics* (Cambridge University Press, Cambridge, 2002).
- [2] A. Onuki and R. A. Ferrell, *Physica (Amsterdam)* **164A**, 245 (1990).
- [3] J. Straub and K. Nitsche, *Fluid Phase Equilib.* **88**, 183 (1993); J. Straub, L. Eicher, and A. Haupt, *Phys. Rev. E* **51**, 5556 (1995).
- [4] H. Boukari *et al.*, *Phys. Rev. A* **41**, 2260 (1990); *Phys. Rev. Lett.* **65**, 654 (1990); R. Allen Wilkinson *et al.*, *Phys. Rev. E* **57**, 436 (1998).
- [5] B. Zappoli *et al.*, *Phys. Rev. A* **41**, 2264 (1990); P. Guenoun *et al.*, *Phys. Rev. E* **47**, 1531 (1993); Y. Garrabos *et al.*, *Phys. Rev. E* **57**, 5665 (1998).
- [6] F. Zhong and H. Meyer, *Phys. Rev. E* **51**, 3223 (1995); **53**, 5935 (1996).
- [7] H. Azuma *et al.*, *Int. J. Heat Mass Transf.* **42**, 771 (1999).
- [8] B. Zappoli *et al.*, *J. Fluid Mech.* **316**, 53 (1996); S. Amiroudine *et al.*, *J. Fluid Mech.* **442**, 119 (2001).
- [9] M. Gitterman and V. Steinberg, *J. Appl. Math. Mech. USSR* **34**, 305 (1971); M. Gitterman, *Rev. Mod. Phys.* **50**, 85 (1978).
- [10] P. Carlès and B. Ugurtas, *Physica (Amsterdam)* **126D**, 69 (1999).
- [11] S. Chandrasekhar, *Hydrodynamic and Hydromagnetic Stability* (Clarendon Press, Oxford, 1961).
- [12] L. D. Landau and E. M. Lifshitz, *Fluid Mechanics* (Pergamon, New York, 1959).
- [13] S. Ashkenazi, Ph.D. thesis, Weizmann Institute of Science, Rehovot, Israel, 1997 (unpublished); S. Ashkenazi and V. Steinberg, *Phys. Rev. Lett.* **85**, 3641 (1999).
- [14] X. Chavanne, Ph.D. thesis, Université Joseph Fourier, Grenoble, 1997 (unpublished).
- [15] X. Chavanne *et al.*, *Phys. Rev. Lett.* **79**, 3648 (1997).
- [16] A. B. Kogan *et al.*, *Phys. Rev. Lett.* **82**, 4635 (1999).
- [17] Andrei B. Kogan and Horst Meyer, *Phys. Rev. E* **63**, 056310 (2001).
- [18] For $0 < \epsilon \ll 1$ the scaling form $\alpha_p = \epsilon^{-\gamma} G(u)$ holds with $u = (\rho/\rho_c - 1)/\epsilon^\beta$. For $|u| \ll 1$ or under Eq. (3) in gravity, we have $G(u) \cong G(0)$ and $\alpha_p \cong G(0)\epsilon^{-\gamma}$.
- [19] For the case of finite Pr , f_λ in Eq. (10) also depends on Pr . Its dependence should become weak once Pr considerably exceeds 1.
- [20] If the initial value of δT has a sufficiently large Fourier component with period $2L$, the two-roll pattern is realized in our simulation even for large Q . In the steady state in the range $42 < Q < 70$ nW/cm², ΔT for two rolls is smaller than that for three rolls by roughly 6%.
- [21] H. Meyer (private communication).